



Efficiency enhancement in PbS/CdS quantum dot-sensitized solar cells by plasmonic Ag nanoparticles

M. A. K. L. Dissanayake¹ · T. Jaseetharan^{1,2,3} · G. K. R. Senadeera^{1,4} · J. M. K. W. Kumari^{1,2}

Received: 28 May 2019 / Revised: 20 August 2019 / Accepted: 4 October 2019 / Published online: 14 November 2019
© Springer-Verlag GmbH Germany, part of Springer Nature 2019

Abstract

Semiconductor quantum dots (Q-dots) are attractive nanomaterials to be used in numerous research areas and device fabrication such as sensors, light-emitting diodes, transistors, and solar cells due to their unique optoelectronic properties. Quantum dot-sensitized solar cells (QDSSCs) have drawn considerable attention due to their cost-effectiveness and ability of multiple exciton generation and tunable energy gap of the quantum dots. In this study, plasmonic Ag colloidal nanoparticle-incorporated plasmonic TiO₂ double-layer (nanofiber/nanoparticle) electrodes have been fabricated. These TiO₂ electrodes were sensitized with PbS/CdS core-shell quantum dots by successive ionic layer adsorption and reaction (SILAR) technique, and QDSSCs were fabricated with polysulfide electrolyte. Cu₂S was formed on brass plate and used as the counter electrode of the QDSSC. A higher power conversion efficiency of 4.09% has been obtained due to the plasmonic effect under the simulated light of 100 mW cm⁻² with AM 1.5 spectral filter. The overall efficiency and short-circuit current density of the plasmonic QDSSC are enhanced by 15% and 23%, respectively, with respect to the QDSSC without Ag nanoparticles. The enhanced performance of the plasmonic QDSSC is evidently due to the enhanced optical absorption by localized surface plasmon resonance effect by the Ag nanoparticles in the TiO₂ photoanode and the resulting increase in the short-circuit photocurrent.

Keywords Quantum dots · Ag nanoparticles · Surface plasmon resonance · Multiple exciton generation · Energy gap

Highlights

- Silver nanoparticle incorporated, PbS:CdS quantum dot-sensitized, photoanode was made
- DSSCs fabricated with above photoanode showed an efficiency of 4.09%
- Efficiency enhancement of 15% and photocurrent enhancement of 23% were achieved due to plasmonic resonance effect

✉ M. A. K. L. Dissanayake
makldis@yahoo.com

¹ National Institute of Fundamental Studies, Hantana Road, Kandy, Sri Lanka

² Postgraduate Institute of Science, University of Peradeniya, Peradeniya, Sri Lanka

³ Department of Physical Sciences, South Eastern University of Sri Lanka, Sammanthurai, Sri Lanka

⁴ Department of Physics, The Open University of Sri Lanka, Nawala, Nugegoda, Sri Lanka

Introduction

Quantum dot-sensitized solar cells (QDSSCs) have gained extensive attention in the area of solar energy conversion devices due to their low production cost and excellent properties of quantum dots such as the ability of multiple exciton generation (MEG), tunable energy gap due to the quantum confinement effect, and high molar extinction coefficients [1, 2]. In a dye-sensitized solar cell (DSSC), dye molecules act as photon absorbers whereas in the case of QDSSC, dye molecules are replaced by the quantum dots. The energy conversion principle of the QDSSC is also similar to the DSSCs with respect to photon absorption, exciton generation, charge carrier injection, and regeneration. However, quantum dots have the ability to create more than one electron-hole pair by a single photon. Photon absorption of quantum dots can be controlled by changing the size of the quantum dots and also by combining different types of quantum dots [3, 4]. Several different

types of QDSSCs have been reported employing several types of semiconductor quantum dots such as CdS, CdS/CdSe, PbS, CdTe, and CdSe/CdS/PbS [4–8]. In these devices, TiO₂ and ZnO semiconductor nanostructures have generally been used to fabricate the photoanodes. Spin coating, ink-jet printing, chemical bath deposition (CBD), and successive ionic layer adsorption and reaction (SILAR) are the commonly used techniques to deposit quantum dots in the semiconductor nanostructures [1, 9, 10].

In order to enhance the performance of the QDSSC, one can modify the structure of the photoanode or the electrolyte or the counter electrode. Usage of different photoanode nanostructures in QDSSCs have been reported. Among them, TiO₂ nanotubes, TiO₂ nanofibers, ZnO nanowires, TiO₂ nanoparticles/nanotubes double layer, and TiO₂ nanoparticles/nanofibers/nanoparticle triple-layer-based photoanodes have attracted much attention during the recent past [11–14]. Several studies have been reported on plasmonic enhancers in organic and inorganic solar cells. The collective oscillations of the free electrons at the surface of a metal nanostructure are known as surface plasmons. Au and Ag plasmonic enhanced InAs/GaAs quantum dot-sensitized solar cells with high efficiency have been reported [15]. In another study, power conversion efficiency of dye-sensitized solar cells has been enhanced up to 7.49% by incorporation of Au plasmonic nanoparticles [16]. Effect of shape and size of plasmonic enhancers have also been studied in organic polymer solar cells [17, 18]. Effect of plasmonic Ag nanocubes has been reported in ZnO nanowire-based PbS quantum dot-sensitized solar cell with an efficiency of 6.03% [19]. Recently, Au plasmonic nanoparticle enhanced PbS quantum dot-sensitized solar cells have been reported with a sixfold efficiency enhancement [20].

In this study, near spherically shaped Ag nanoparticles were synthesized and characterized. PbS/CdS core-shell structure quantum dot-based TiO₂ nanofiber/nanoparticle double-layer photoanodes have been fabricated with and without synthesized Ag plasmonic nanoparticles. QDSSCs were fabricated with liquid-based polysulfide electrolyte, and the effect of localized surface plasmon resonance of Ag nanoparticle on photocurrent has been studied. As far as we are aware, this is the first report of using Ag nanoparticles in a DSSC sensitized with PbS/CdS core-shell semiconductor Qdots incorporated into a double-layer TiO₂ photoanode structure consisting of TiO₂ nanoparticles and TiO₂ nanofibers aimed at enhancing light absorption by multiple effects.

Experimental

Materials

Fluorine-doped tin oxide (FTO)-coated glass ($8 \Omega \text{ cm}^{-2}$, Solaroix), Triton X-100 (Sigma-Aldrich), titanium(IV) isopropoxide (97%, Fluka), propan-1-ol (99.9%, Fisher), glacial acetic acid (99%, Fisher), titanium dioxide P90 powder (Evonik), titanium dioxide powder P25 (Degussa), hydrochloric acid (37%, Sigma-Aldrich), polyethylene glycol (99.8%, Sigma-Aldrich), methanol (99.8%, Sigma-Aldrich), trisodium citrate dihydrate (99%, Sigma-Aldrich), sulfur (99%, Daejng), silver nitrate (> 99, Sigma-Aldrich), potassium chloride (99%, Aldrich), N,N-dimethyl formamide (99%, Sigma-Aldrich), sodium sulfide hydrate (> 60%, Sigma-Aldrich), cadmium(II) chloride (99.99%, Sigma-Aldrich), and lead(II) nitrate (99%, Sigma-Aldrich) were used as received without any modification.

Synthesis of Ag nanoparticles

Ag colloidal nanoparticles (NPs) were synthesized by the citrate reduction method. Initially, 0.1 g of trisodium citrate dihydrate was dissolved in 10 ml deionized water. One milliliter of this solution was added to the boiled 1 mM silver nitrate aqueous solution, and the mixture was continuously stirred until the solution became deep orange in color. Then, the resulting Ag nanoparticle colloidal solution was allowed to cool down to room temperature.

Preparation of TiO₂ double-layered photoanode

TiO₂ compact layer (CL) was first deposited on precleaned, fluorine-doped, tin oxide (FTO) glass substrates by spin coating using precursor solution prepared from titanium(IV) isopropoxide. The solution was spin coated for 1 min with 3000 rpm. The substrate was then sintered at 450 °C for 45 min. In order to make the CL pinhole-free, TiO₂ P90 paste was prepared with 0.25 g of TiO₂ P90 powder and 1 ml of HNO₃ and spin coated on the FTO/TiO₂ CL with 3000 rpm for 1 min, and the electrode was again sintered at 450 °C for 45 min and then allowed to cool to room temperature. A TiO₂ P25 nanoparticle paste was prepared with 0.25 g of TiO₂ P25 powder, 0.05 g of polyethylene glycol, 1 drop of Triton X-100, and 1 ml of 0.1 M HNO₃. TiO₂ P25 nanoparticle paste with Ag nanoparticles was deposited on electrode FTO/TiO₂ CL/TiO₂ P90 by doctor blading method on TiO₂ P90 layer, and the resulting FTO/TiO₂

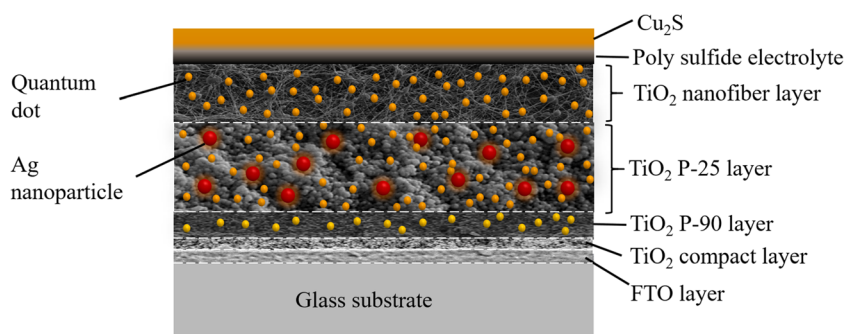
CL/TiO₂ P90/TiO₂ P25 composite electrode was sintered at 450 °C for 45 min. Finally, on top of the TiO₂ P25 nanoparticle layer, a TiO₂ nanofiber (NF) layer was electrospun and the composite FTO/TiO₂ CL/TiO₂ P90/TiO₂ P25/TiO₂ NF photoanode was sintered at 450 °C for 45 min.

For the synthesis of TiO₂ nanofiber (NF) layer, a precursor solution containing 0.75 g of polyvinyl acetate, 1.5 ml of titanium(IV) isopropoxide, 0.5 ml of glacial acetic acid, and 9.5 ml of N,N-dimethylformamide (DMF) was electrospun on the FTO/CL/TiO₂ P90/TiO₂ P25 layer using electrospinning technique (NaBond Technologies, Hong Kong). During the electrospinning, rate of solution flow was kept at a constant value of 2 ml/h. The potential difference and distance between the spray gun and TiO₂ electrodes were kept at 20 kV and 6.5 cm, respectively. Electrospinning process was continued up to 20 min for an optimized thickness of nanofiber layer, and FTO/CL/TiO₂ P90/TiO₂ P25/TiO₂ NF electrodes were sintered at 450 °C for 45 min. Amount of Ag nanoparticles was optimized by testing preliminary test solar cells and that optimized amount of Ag colloidal solution was incorporated to the TiO₂ electrodes.

Incorporation of PbS/CdS core-shell quantum dots

Incorporation of PbS/CdS core-shell quantum dots in to the TiO₂ nanostructure (TiO₂ CL/TiO₂ P90/TiO₂ P25/TiO₂ NF) was done by using SILAR method. In order to get a higher efficiency, number of SILAR cycles were optimized for PbS/CdS combination. For the deposition of PbS quantum dots, aqueous solutions of 0.1 M Pb(NO₃)₂ and 0.1 M Na₂S were used as cationic and anionic precursor solutions. Two SILAR cycles were done with 1 min per each dipping for PbS quantum dots. For the deposition of CdS quantum dot shell structure over the PbS quantum dots, aqueous solutions of 0.1 M CdCl₂ and 0.1 M Na₂S were used as cationic and anionic precursor solutions. Four SILAR cycles were done with 1 min per each dipping for CdS quantum dots. Finally, the photoanodes were dried at 80 °C.

Fig. 1 Schematic diagram of a quantum dot-sensitized, plasmonic solar cell with a TiO₂ nanoparticle/nanofiber double-layer photoanode structure



Preparation of the electrolyte

Liquid polysulfide electrolyte was prepared by the following method. Sulfur (2 M), 2 M Na₂S, and 0.2 M KCl were dissolved in a mixture of deionized water and methanol in the ratio of 3:7 (v/v). The mixture was continuously stirred until a clear solution was obtained.

Preparation of the counter electrode

A 2 cm × 1 cm brass plate was cleaned by dipping it in concentrated HCl at 80 °C. Cleaned surface was masked leaving a 6 mm × 6 mm area. Cu₂S was formed on the unmasked area by applying appropriate amount of polysulfide electrolyte.

Fabrication of QDSSC

Cu₂S counter electrode was placed on the effective area of the photoanode, and appropriate amount of polysulfide electrolyte was injected between the two electrodes. Both electrodes were held together by using steel clips. A schematic diagram of the structure of the plasmonic-enhanced TiO₂ nanoparticle/nanofiber double-layer-based quantum dot-sensitized solar cell is shown in Fig. 1.

Characterizations

Surface morphology of the electrodes and nanoparticles were examined by using ZEISS EVO Scanning Electron Microscope and JEOL JEM-2100 high-resolution transmission electron microscope (HRTEM) with an accelerating voltage of 200 kV. Energy-dispersive X-ray (EDX) spectra were obtained from Ametek EDAX module with Octane T Optima-60 EDX detector in TEM mode. Optical absorption spectra were obtained by Shimadzu 2450 UV–Vis spectrophotometer in the wavelength interval from 350 to 1100 nm. Current–voltage characterization of each QDSSC were done under simulated light of 100 mW cm⁻² with AM 1.5 filter using a computer-controlled multi-meter (Keithley 2000 model) coupled

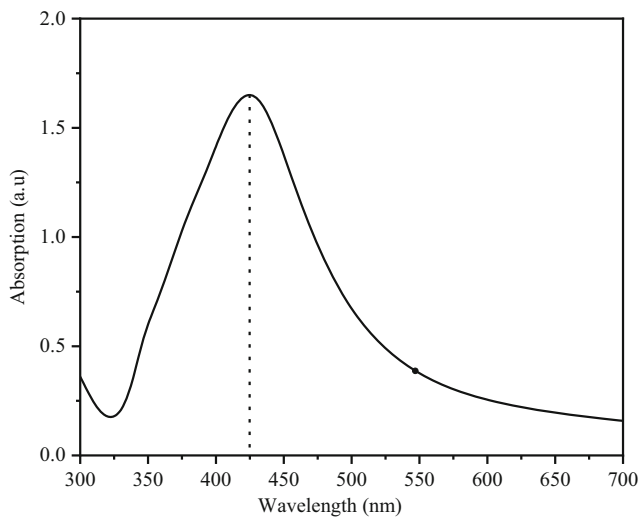
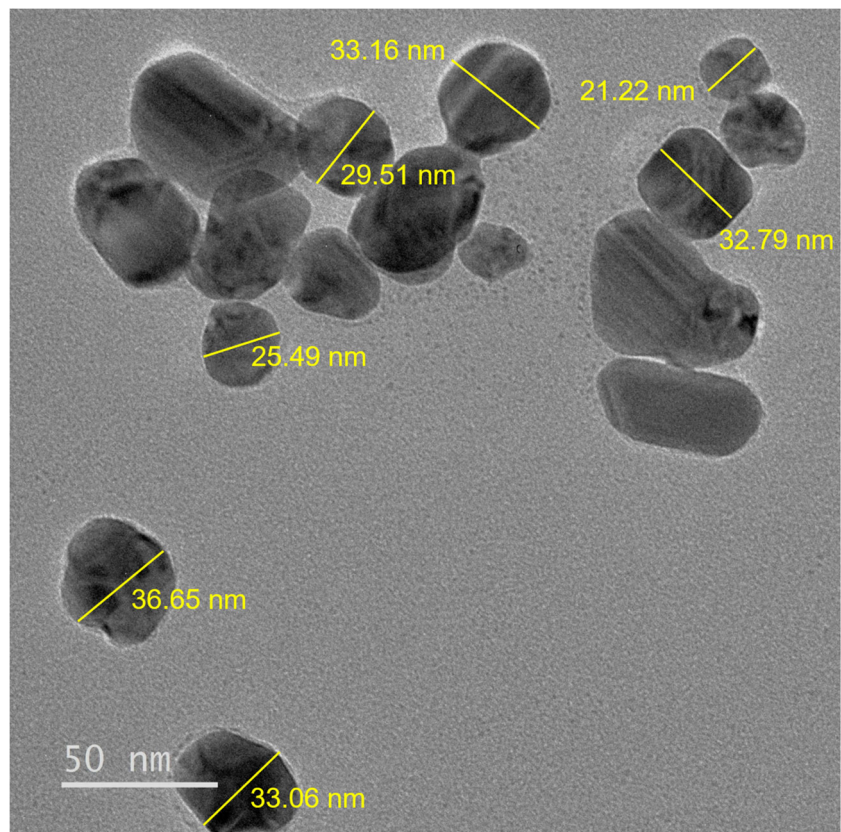


Fig. 2 Optical absorption spectrum of synthesized Ag colloidal nanoparticles

with potentiostat/galvanostat unit (HA-301). The effective area of the QDSSC was 0.25 cm^2 . In order to study the interface resistances of the QDSSCs, impedance spectra of each QDSSC was obtained by performing electrochemical impedance spectroscopy (EIS) under the simulated light of 100 mW cm^{-2} with AM 1.5 spectral filter by using Autolab potentiostat/galvanostat PGSTAT128 N with a frequency response analyzer (Metrohm) in the frequency between 0.01 Hz and 1 MHz.

Fig. 3 TEM image of synthesized Ag nanoparticles



Results and discussion

Figure 2 shows the absorption spectrum of the colloidal Ag nanoparticles. It shows a broad absorption in the visible region having a maximum around 425 nm. The average size of the Ag nanoparticles was estimated by using the wavelength corresponds to the absorption peak maximum and found to be in between 30 and 40 nm [21]. This was further confirmed by the HRTEM.

Figure 3 displays the TEM image of the Ag nanoparticles. According to the TEM image, average size of the Ag nanoparticles is between 30 and 40 nm in agreement with the average particle size calculated based on the optical absorption spectrum.

Figure 4 shows the EDX spectrum of the TiO_2 electrode containing Ag nanoparticles. Confirming the existence of the Ag nanoparticles. According to the EDX data, amount of the Ag nanoparticle in the TiO_2 electrode is estimated to be 0.36% (by weight).

Figure 5 displays the optical absorption spectra of TiO_2 double-layered electrode (curve 1) and TiO_2 double-layered electrode with Ag nanoparticles and PbS/CdS quantum dots (curve 2). Clearly curve 2 shows enhancement in optical absorption throughout the entire wavelength region due to the incorporation of CdS and PbS in the photoanode. The contribution from plasmonic effect due to Ag nanoparticles is clearly visible in the broadened spectrum in the 350 to 550 nm region in

Fig. 4 EDX spectrum of the TiO₂ electrode with Ag nanoparticles

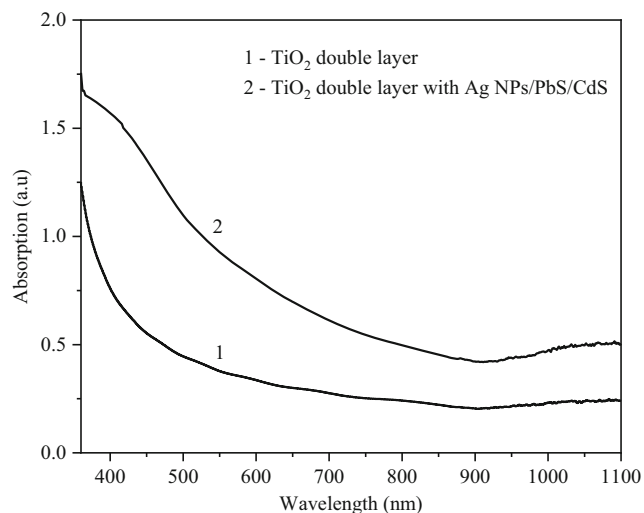
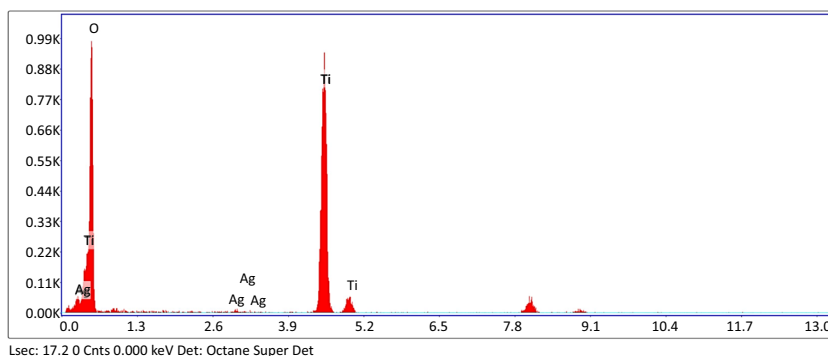


Fig. 5 UV–Vis absorption spectra of TiO₂ double layer (curve 1) and Ag nanoparticle incorporated TiO₂ double layer sensitized with PbS/CdS quantum dots (curve 2)

agreement with Fig. 2 [21, 22]. The contribution from PbS is clearly shown as a broadened peak in the near infrared region from 900 to 1100 nm [14].

Figure 6 displays the surface morphology of the TiO₂ nanoparticle layer and TiO₂ nanofiber layer. Nanofibers are expected to enhance the light absorption by multiple scattering effects within the nanofiber structure and by the interface between the nanofiber/nanoparticle layer as already reported previously by our group [14, 23, 24].

Fig. 6 Surface SEM images of the TiO₂ nanoparticle layer (left) and TiO₂ nanofiber layer (right)

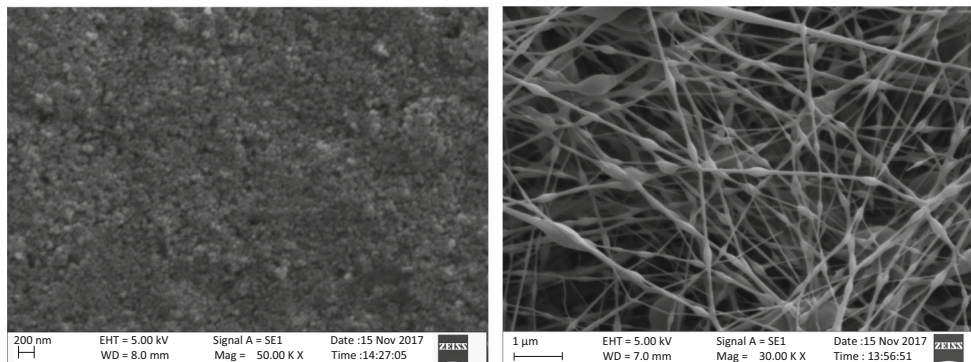


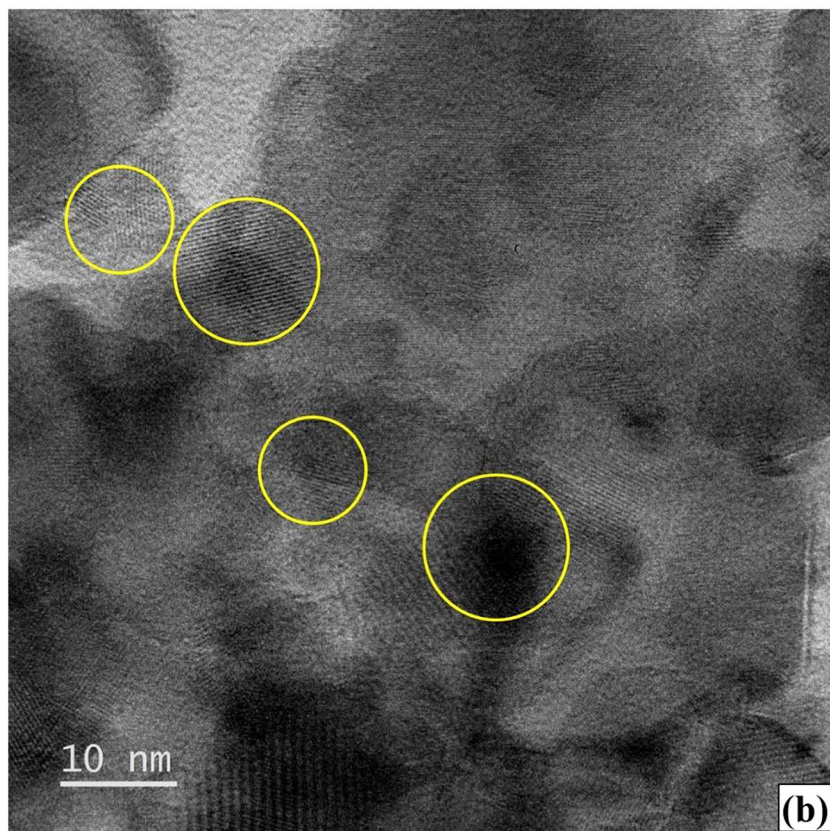
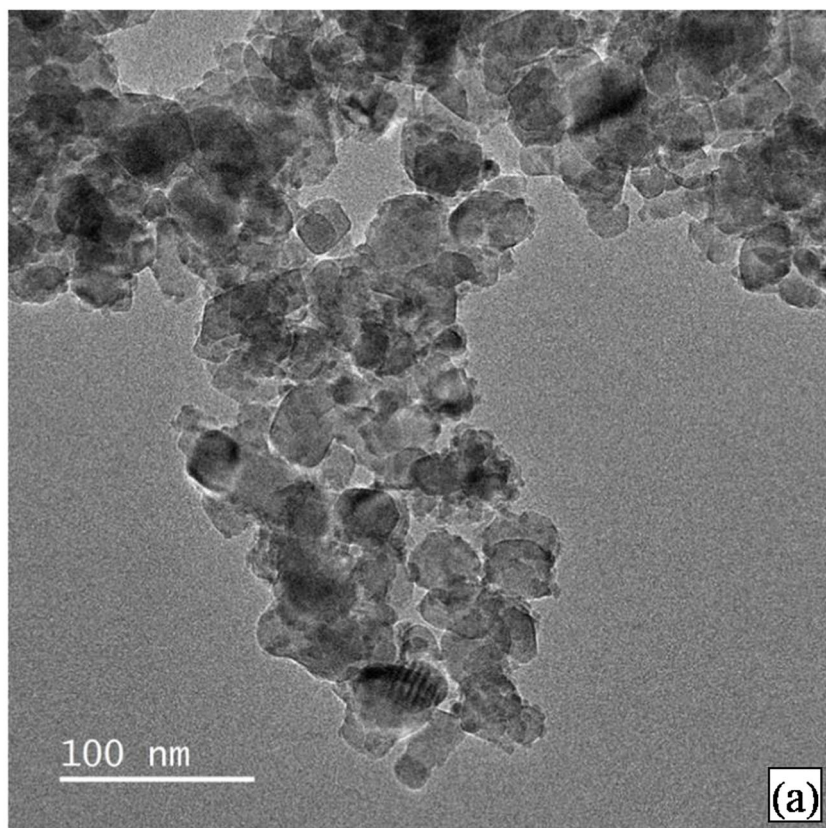
Figure 7 shows the morphology of the PbS/CdS quantum dots in the TiO₂ nanostructure. This proves the presence of PbS/CdS quantum dots in the photoanode. Previously, HRTEM images with very similar features have also been reported by several other researchers confirming the presence of the different combinations of quantum dots in this way [25, 26].

Figure 8 represents the EDX elemental maps of Ti, Ag, Pb, Cd, and S of the photoanode, and Fig. 9 displays the corresponding EDX spectra of the photoanode. This confirms the existence of quantum dots and Ag nanoparticles in the TiO₂ photoanode.

Variation of power conversion efficiency of the solar cells with number of SILAR cycles is given in Table 1. Photoanode sensitized with 2 SILAR cycles of PbS and 4 SILAR cycles of CdS shows better efficiency. When the number of PbS SILAR cycles increased beyond 2, the efficiency decreases as it occupies available nanoporous space in the TiO₂ electrode and not enough space is available for the formation of PbS/CdS quantum dots. When CdS SILAR cycle increases beyond 4, the efficiency decreases due to the increased thickness of the shell which obstructs the electron transfer through the shell.

Current–voltage characterization is an important measurement to evaluate the performance of the solar cells which gives the photovoltaic parameters of the solar cells. Power conversion efficiency can be calculated using the following equation.

Fig. 7 **a** TEM and **b** HRTEM images of the PbS/CdS quantum dots incorporated in the TiO₂ nanostructure photoanode



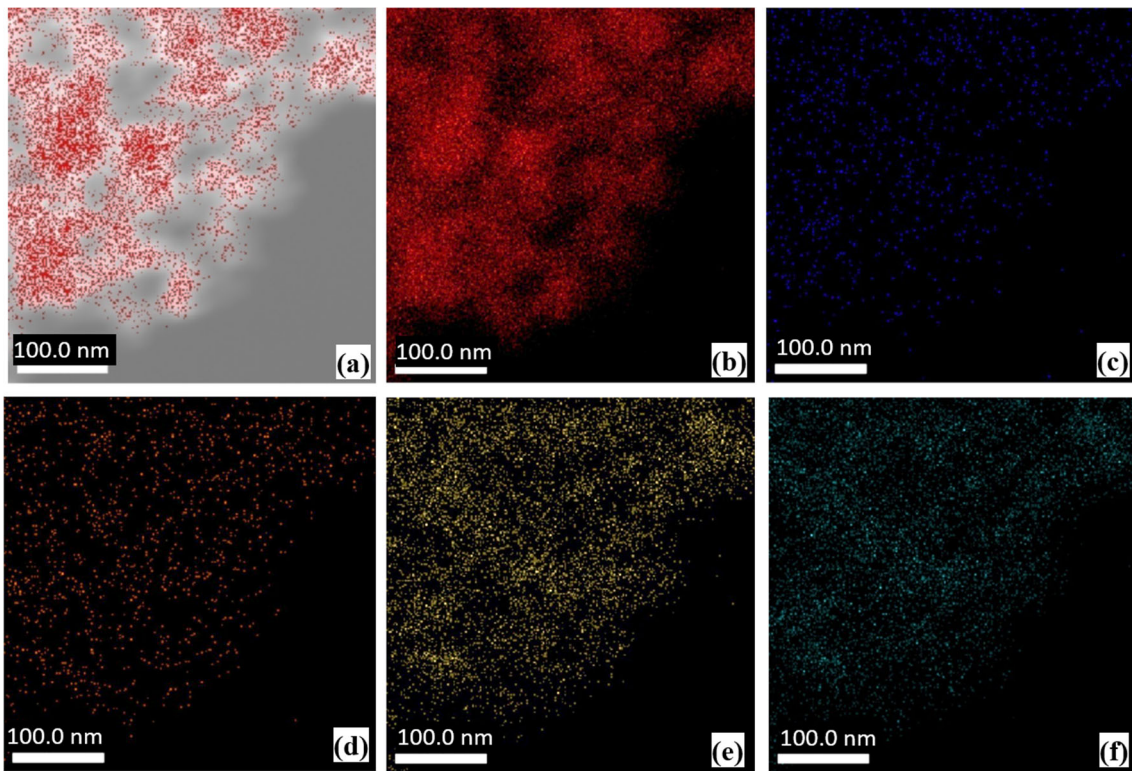


Fig. 8 a Selected area for mapping and elemental mapping of b Ti, c Ag, d Pb, e Cd, and e S

$$\eta = \frac{J_{SC} \cdot V_{OC} \cdot FF}{P_{IN}} \times 100\%$$

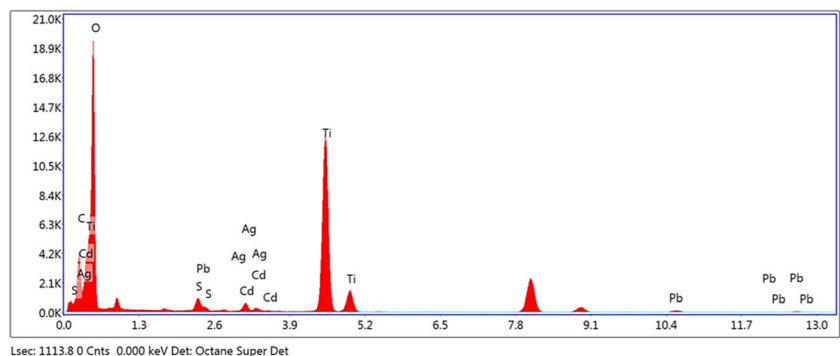
where V_{OC} is the open-circuit voltage, J_{SC} is the short-circuit current density, FF is the fill factor, and P_{IN} is the incident power density.

In a QDSSC, semiconductor quantum dots behave as light absorbers or sensitizers and create excited electron-hole pairs or excitons. In this study, PbS and CdS act as such sensitizers. Figure 10 depicts the mechanism of the PbS/CdS quantum dot-sensitized solar cell.

According to the schematic diagram of the PbS/CdS QDSSC, PbS quantum dots absorb photons in the near-infrared region and CdS quantum dots absorb photons in the

visible region. Both quantum dots create the electron-hole pairs. Electrons in the conduction band of the CdS are transferred to the conduction bands of the PbS and TiO₂. Electrons in the conduction band of the PbS are transferred in to the conduction band of the TiO₂. Due to this mechanism, electrons are injected to the conduction band of TiO₂ from PbS/CdS quantum dots. These electrons are transferred through the FTO and external circuit and reached the Cu₂S counter electrode. Due to the action of the polysulfide redox couple, the quantum dots are regenerated [27, 28]. In the presence of Ag nanoparticle, it collects the photons by LSPR effect and generates a strong oscillating electric field. This localized electric field enhances the photocurrent by exciting electrons [29].

Fig. 9 EDX spectrum of the composite TiO₂ photoanode

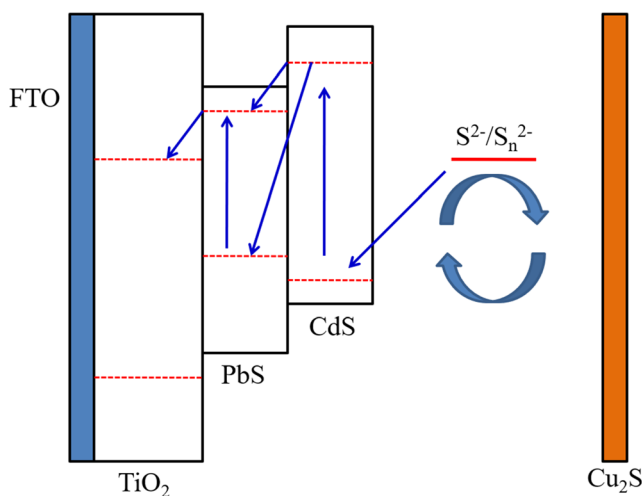
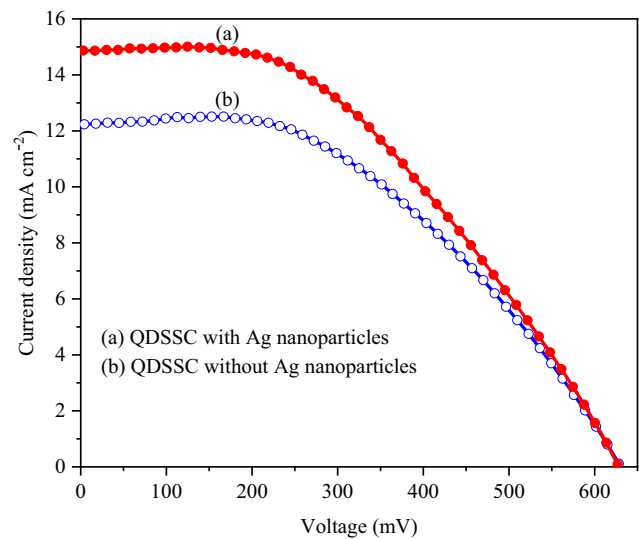


Lsec: 1113.8 0 Cnts 0.000 keV Det: Octane Super Det

Table 1 Variation of efficiency of QDSSCs with different number of SILAR cycles

SILAR cycles for PbS	SILAR cycles for CdS	Current density (mA cm^{-2})	Efficiency (%)
2	0	8.32	1.52 ± 0.09
2	1	9.12	2.13 ± 0.12
2	2	10.53	2.86 ± 0.17
2	3	11.48	3.41 ± 0.08
2	4	12.07	3.55 ± 0.11
2	5	11.96	3.48 ± 0.07
3	0	8.56	2.02 ± 0.19
3	1	9.04	2.98 ± 0.21
3	2	10.24	3.01 ± 0.16
3	3	11.01	3.12 ± 0.23
3	4	10.11	3.28 ± 0.18
3	5	9.89	3.06 ± 0.07

Figure 11 exhibits the current–voltage characteristics of the QDSSCs fabricated with TiO_2 double-layer photoanode structure and Ag nanoparticle incorporated TiO_2 double-layer photoanode structure under the simulated light of 100 mW cm^{-2} with AM 1.5 spectral filter. The Ag nanoparticle incorporated nanostructure-based QDSSC shows better performance. This is evidently due to the efficient light absorption by localized surface plasmon resonance (LSPR) of Ag nanoparticles as reported by many previous studies [15, 19, 29]. When the frequency of the incident photons matches with the frequency of free electrons on the surface of metal nanostructures, it will lead to collective oscillations of the electrons and this oscillation is defined as localized surface plasmon resonance. Frequency of the LSPR is determined by size and shape of the plasmonic nanostructure, interparticle distance, amount of the particles,

**Fig. 10** Schematic diagram of the PbS/CdS-sensitized solar cells**Fig. 11** Current–voltage characteristics of PbS/CdS quantum dot-sensitized solar cells

and dielectric constant of the surrounding material [30] (Table 2).

According to these observations, the overall efficiency and short-circuit current density of the QDSSC are enhanced by 15% and 23%, respectively, due to the plasmonic effect. Plasmonic nanoparticles involve scattering process, and absorption in solar cells depends on the size and shape of the nanoparticles. According to literature, plasmonic nanoparticles of less than 50 nm size are expected to make a significant contribution to the light absorption process [31, 32]. Average size of synthesized Ag nanoparticles in this study is estimated to be between 30 and 40 nm. In a QDSSC, quantum dots behave as light absorbers creating excitons. In the presence of plasmonic Ag nanoparticle, it collects the

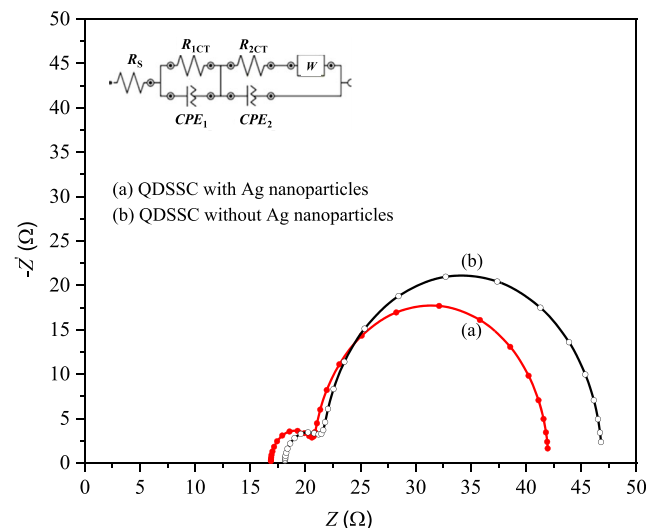
**Fig. 12** Nyquist plots of PbS/CdS quantum dot-sensitized solar cells under simulated light of 100 mW cm^{-2} with AM 1.5 filter

Table 2 Photovoltaic parameters of PbS/CdS QDSSCs

Photoanode	J_{SC} (mA cm ⁻²)	V_{OC} (mV)	FF (%)	Efficiency (%)
Without Ag NPs	12.07	630.0	46.67	3.55 ± 0.11
With Ag NPs	14.85	627.7	43.90	4.09 ± 0.17

photons by LSPR effect and generate a strong oscillating electric field. This localized electric field enhances the photocurrent by exciting electrons in the sensitizers [20]. Therefore, Ag nanoparticles have clearly contributed to the optical absorption process and enhanced the performance of the QDSSC by increasing the short-circuit photocurrent.

From the electrochemical impedance measurements, Nyquist plots with Z' versus Z were obtained for the QDSSCs as mentioned before. Nyquist plots of each QDSSC were analyzed by fitting the parameters with an equivalent circuit using NOVA 1.11 analyzing software, and series resistance and interface resistances were estimated. Figure 12 displays the Nyquist plots of the QDSSCs obtained from the impedance measurements with an equivalent circuit. As it is well established that the smaller semicircle appears in the higher frequency region is ascribed to the charge transfer resistance (R_{1CT}) of the electrolyte/counter electrode interface. The larger semicircle in the intermediate frequency region is associated to the charge transfer resistance (R_{2CT}) of the quantum dot-loaded TiO₂ electrode/electrolyte interface R_s is the series resistance of the devices and CPE₁ and CPE₂ are the constant phase elements and W is the finite Warburg impedance element [33].

Estimated electrochemical impedance parameters which were obtained from the equivalent circuit fitting are listed in Table 3. Ag nanoparticle incorporated photoanode shows a lower series resistance R_s and a lower charge transfer resistance (R_{1CT}) compared to the controlled QDSSC leading to an efficient electron transfer at the photoanode/electrolyte interface and thereby enhancing the photocurrent. Bode phase plots of the QDSSCs are displayed in Fig. 13. Electron lifetimes can be calculated using the following equation.

Table 3 Electrochemical impedance parameters of the QDSSCs

Photoanode	R_s (Ω)	R_{1CT} (Ω)	R_{2CT} (Ω)
Without Ag NPs	18.1	25.3	9.5
With Ag NPs	16.9	6.4	21.2

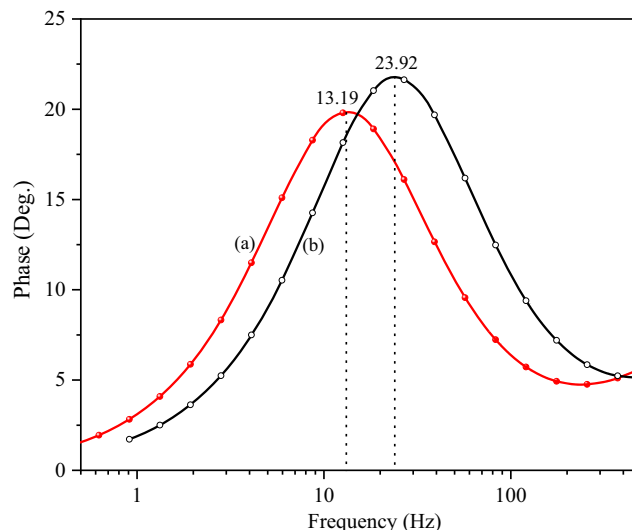


Fig. 13 Bode plots of QDSSC (a) with Ag nanoparticles and (b) without Ag nanoparticles

$$\tau = \frac{1}{2\pi f_{max}}$$

f_{max} values are obtained from the Bode phase plots. Calculated life time (τ) values are given in Table 4.

The electrons in the Ag incorporated photoanode have longer lifetime which reduces the recombination compared to the controlled electrode. Electrons can effectively transfer with less recombination resulting in a higher short-circuit current [34].

Conclusions

We have fabricated solar cells with TiO₂ nanofiber/TiO₂ nanoparticle double-layer photoanode sensitized with PbS/CdS core-shell structure. To enhance the efficiency of these QDSSCs further, we have synthesized colloidal Ag nanoparticles and incorporated into the TiO₂ nanostructure. These plasmonic QDSSCs exhibit a high efficiency of 4.09% which can clearly be attributed to the enhanced optical absorption by localized surface plasmon resonance effect by the Ag nanoparticles in the TiO₂ photoanode coupled with improved light absorption by multiple scattering effect due to the double-layer TiO₂ photoanode. Both these factors have increased the short-circuit photocurrent.

Table 4 Comparison of electron lifetime and photovoltaic parameters of QDSSCs

Photoanode	τ (ms)	J_{SC} (mA cm ⁻²)	Efficiency (%)
Without Ag NPs	6.65	12.07	3.55 ± 0.11
With Ag NPs	12.07	14.85	4.09 ± 0.17

Funding information This study is financially supported by the National Science Foundation of Sri Lanka under grant number NSF/SCH/2018/04.

References

- Tang J, Sargent EH (2011) Infrared colloidal quantum dots for photovoltaics: fundamentals and recent progress. *Adv Mater* 23(1):12–29
- Nozik AJ, Beard MC, Luther JM, Law M, Ellingson RJ, Johnson JC (2010) Semiconductor quantum dots and quantum dot arrays and applications of multiple exciton generation to third-generation photovoltaic solar cells. *Chem Rev* 110(11):6873–6890
- Kongkanand A, Tvrdy K, Takechi K, Kuno M, Kamat PV (2008) Quantum dot solar cells. Tuning photo response through size and shape control of CdSe-TiO₂ architecture. *J Am Chem Soc* 130(12):4007–4015
- Lang Lee Y, Lo YS (2009) Highly efficient quantum-dot-sensitized solar cell based on co-sensitization of CdS/CdSe. *Adv Funct Mater* 19:604–609
- Shalom M, Dor S, Grinis L, Zaban A (2009) Core/CdS quantum dot/shell mesoporous solar cells with improved stability and efficiency using an amorphous TiO₂ coating. *J Phys Chem C* 113:3895–3898
- Zhao N, Osedach TP, Chang LY, Geyer SM, Wanger D, Binda MT, Arango AC, Bawendi MG, Bulovic V (2010) Colloidal PbS quantum dot solar cells with high fill factor. *ACS Nano* 4(7):3743–3752
- Bang JH, Kamat PV (2009) Quantum dot sensitized solar cells. A tale of two semiconductor nanocrystals: CdSe and CdTe. *ACS Nano* 3(6):1467–1476
- Raj CJ, Karthick SN, Park S, Hemalatha KV, Kim S-K, Prabakar K, Kim H-J (2014) Improved photovoltaic performance of CdSe/CdS/PbS quantum dot sensitized ZnO nanorod array solar cell. *J Power Sources* 248:439–446
- Chang C-H, Lee Y-H (2007) Chemical bath deposition of CdS quantum dots onto mesoscopic TiO₂ films for application in quantum-dot-sensitized solar cells. *J App Phys Lett* 91:053503
- Pathan HM, Sankapal BR, Desai JD, Lokhande CD (2002) Preparation and characterization of nanocrystalline CdSe thin films deposited by SILAR method. *Mater Chem Phys* 78:11–14
- Sun W-T, Yu Y, Pan X-Y, Gao X-F, Chen Q, Peng LM (2008) CdS quantum dots sensitized TiO₂ nanotube-array photoelectrodes. *J Am Chem Soc* 130(4):1124–1125
- Sudhagar P, Jung JH, Park S, Lee YG, Sathyamoorthy R, Kang YS, Ahn H (2000) The performance of coupled (CdS:CdSe) quantum dot-sensitized TiO₂ nanofibrous solar cells. *Electrochem Commun* 11:2220–2224
- Jean J, Chang S, Brown PR, Cheng JJ, Rekemeyer PH, Bawendi MG, Gradedecak S, Bulović V (2013) ZnO nanowire arrays for enhanced photocurrent in PbS quantum dot solar cells. *Adv Mater* 25(20):2790–2796
- Dissanayake MAK, Jaseetharan T, Senadeera GKR, Thotawatthage CA (2018) A novel, PbS:Hg quantum dot-sensitized, highly efficient solar cell structure with triple layered TiO₂ photoanode. *Electrochim Acta* 269:172–179
- Wu J, Mangham SC, Reddy VR, Manasreh MO, Weaver BD (2012) Surface plasmon enhanced intermediate band-based quantum dots solar cell. *Sol Energy Mater Sol Cells* 102:44–49
- Dao V-D, Choi H-S (2016) Highly-efficient plasmon-enhanced dye-sensitized solar cells created by means of dry plasma reduction. *Nanomaterials* 6:70
- Notarianni M, Vernon K, Chou A, Aljada M, Liu J, Motta N (2014) Plasmonic effect of gold nanoparticles in organic solar cells. *Sol Energy* 106:23–37
- Li X, Choy WCH, Lu H, Sha WEI, Ho AHP (2013) Efficiency enhancement of organic solar cells by using shape-dependent broadband plasmonic absorption in metallic nanoparticles. *Adv Funct Mater* 23:2728–2735
- Kawawaki T, Wang H, Kubo T, Saito K, Nakazaki J, Segawa H, Tatsuma T (2015) Efficiency enhancement of PbS quantum dot/ZnO nanowire bulk-heterojunction solar cells by plasmonic silver nanocubes. *ACS Nano* 9:4165–4172
- Kawawaki T, Tatsuma T (2013) Enhancement of PbS quantum dot-sensitized photocurrents using plasmonic gold nanoparticles. *Phys Chem Chem Phys* 15(46):20247–20251
- Dadosh T (2009) Synthesis of uniform silver nanoparticles with a controllable size. *Mater Lett* 63:2236–2238
- Brennan TP, Ardalan P, Lee H-B-R, Bakke JR, Ding IK, McGehee MD, Bent SF (2011) Atomic layer deposition of CdS quantum dots for solid-state quantum dot sensitized solar cells. *Adv Energy Mater* 1:1169–1175
- Dissanayake MAK, Divarathna HKDWMN, Dissanayake CB, Senadeera GKR, Ekanayake PMPC, Thotawatthage CA (2016) An innovative TiO₂ nanoparticle/nanofibre/nanoparticle, three-layer composite photoanode for efficiency enhancement in dye-sensitized solar cells. *J Photochem Photobiol A Chem* 322:110–118
- Dissanayake MAK, Sarangika HNM, Senadeera GKR, Divarathna HKDWMNR, Ekanayake EMPC (2017) Application of a nanostructured, tri-layer TiO₂ photoanode for efficiency enhancement in quasi-solid electrolyte-based dye-sensitized solar cells. *J Appl Electrochem* 47:1239–1249
- Bhand GR, Chauré NB (2017) Synthesis of CdTe, CdSe and CdTe/CdSe core/shell QDs from wet chemical colloidal method. *J Mater Sci Semicond Process* 68:279–287
- Huang K-Y, Luo Y-H, Cheng H-M, Tang J, Huang JH (2019) Performance enhancement of CdS/CdSe quantum dot-sensitized solar cells with (001)-oriented anatase TiO₂ nanosheets photoanode. *Nanoscale Res Lett* 14:18
- González-Pedro V, Sima C, Marzari G, Boix PP, Giménez S, Shen Q, Dittich T, Mora-Seró I (2013) High performing PbS quantum dot sensitized solar cells exceeding 4% efficiency: the role of metal precursor in the electron injection and charge separation. *J Phys Chem Chem Phys* 15:13835–13843
- Thulasi-Varma CV, Srinivasa Rao S, Ikkurthi KD, Kim S-K, Kang T-S, Kim H-J (2015) Enhanced photovoltaic performance and morphological control of the PbS counter electrode grown on functionalized self-assembled nanocrystals for quantum-dot sensitized solar cells via cost-effective chemical bath deposition. *J Mater Chem C* 3:10195–10206
- Dissanayake MAK, Kumari JMKW, Senadeera GKR, Thotawatthage CA (2015) Efficiency enhancement in plasmonic dye-sensitized solar cells with TiO₂ photoanodes incorporating gold and silver nanoparticles. *J Appl Electrochem* 46:47–58
- Ye W, Long R, Huang H, Xiong Y (2017) Plasmonic nanostructures in solar energy conversion. *J Mater Chem C* 5:1008–1021
- Pillai S, Green MA (2010) Plasmonics for photovoltaic applications. *Sol Energy Mater Sol Cells* 94:1481–1486
- Smith JG, Fauchaux JA, Jain PK (2015) Plasmon resonances for solar energy harvesting: A mechanistic outlook. *Nano Today* 10:67–80
- Wang Q, Moser JE, Gratzel M (2005) Electrochemical impedance spectroscopic analysis of dye-sensitized solar cells. *J Phys Chem B* 109:14945–14953
- Mingsukang MA, Buraidah MH, Careem MA (2017) Development of gel polymer electrolytes for application in quantum dot-sensitized solar cells. *Ionics* 23:347–355

Publisher's note Springer Nature remains neutral with regard to jurisdictional claims in published maps and institutional affiliations.